RSC Advances

PAPER

View Article Online
View Journal | View Issue



Cite this: *RSC Adv.*, 2018, **8**, 12282

# Amine-functionalized MIL-53(Al) with embedded ruthenium nanoparticles as a highly efficient catalyst for the hydrolytic dehydrogenation of ammonia borane†

Shuren Zhang, Liqun Zhou* and Menghuan Chen

Received 18th February 2018
Accepted 26th March 2018

DOI: 10.1039/c8ra01507d

rsc.li/rsc-advances

Well-dispersed ruthenium nanoparticles (Ru NPs) are immobilized within the pores of amine-functionalized MIL-53 *via* an *in situ* impregnation-reduction method. The resulting Ru/MIL-53(Al)-$NH_2$ catalyst exhibits superior catalytic performance for the dehydrogenation of ammonia borane (AB) at ambient temperature relative to the Ru/MIL-53(Al) catalyst; it has a turnover frequency (TOF) of 287 mol $H_2$ $min^{-1}$ (mol Ru)$^{-1}$ and an activation energy ($E_a$) of 30.5 kJ $mol^{-1}$. The amine groups present in the MIL-53(Al)-$NH_2$ framework facilitate the formation and stabilization of ultra-small Ru NPs by preventing their aggregation. Additionally, the Ru/MIL-53(Al)-$NH_2$ catalyst exhibits satisfactory durability and reusability: 72.4% and 86.3% of the initial catalytic activity was maintained after the fifth successive cycle of the hydrolytic dehydrogenation of AB in the two respective tests.



## Introduction

Hydrogen has great potential as a clean energy carrier to facilitate the transition from non-renewable fossil fuels to renewable and environmentally friendly energy sources.[1,2] However, the exploitation of suitable hydrogen storage materials remains a challenge.[3]

Ammonia borane ($NH_3BH_3$, AB), a minimally toxic, environmentally friendly chemical reagent, has been identified as a promising hydrogen storage material with high hydrogen content (19.6%), stability under ambient conditions, high solubility, and a controllable hydrogen release rate.[4,5] In particular, the hydrolysis of AB by an appropriate catalyst can release 3 mol of hydrogen per mol of AB, and thus AB is believed to be the most convenient portable hydrogen storage material identified to date.[6] Thus, the development of a high-performance catalyst for the hydrolysis of AB is highly desirable.

Metal organic frameworks (MOFs) are a new category of hybrid materials constructed of metal centers and organic ligands.[7] Due to their high specific surface areas, variety of structures, and chemical stability, MOFs have drawn increasing attention for applications in drug delivery, gas adsorption, and catalytic reactions.[8–10] The facile functionalization of the internal pore surface is another important characteristic of MOFs.[11] To date, a series of functionalized MOFs that incorporate a variety of functional groups (*e.g.*, –OH and –$NH_2$) has been successfully prepared.[12,13] Among them, amine groups have attracted the most attention from researchers due to their ability to function as interaction sites for supported metallic nanoclusters in heterogeneous catalysis.[14] In addition, functionalization with aromatic –$NH_2$ groups may facilitate metal complex binding, as demonstrated by M. J. Ingleson *et al.*[15] However, the utilization of these functionalized MOFs as catalysts in the dehydrogenation of AB aqueous solution has rarely been reported.

Recently, supported metal nanoparticles (NPs) have been extensively used in the hydrolysis of AB,[16] and increasing attempts have been devoted to encapsulating well-distributed and ultra-small metal NPs within MOF materials. In previous studies, researchers focused on immobilizing bimetallic or trimetallic alloy NPs in matrixes to improve the catalysis of AB hydrolysis through the synergistic effects of metal NPs, such as CuNi/MIL-101,[17] RuCo/MIL-96,[18] RuCuCo/MIL-101,[19] and $Ag_{30}Pb_{70}$/C.[20] However, no studies have described the impact of amine-functionalized MOFs on AB hydrolysis. In this work, as a supporting material for metal loading, amine-functionalized MOFs may prove to be an effective strategy for the design and development of highly active hybrid materials for achieving high catalytic hydrogen generation from AB hydrolysis, and also offers a helpful overview of the exploration of stable and efficient MOF-based catalysts for solving various global environmental and energy problems.

*Hubei Collaborative Innovation Center for Advanced Organic Chemical Materials, Ministry of Education Key Laboratory for the Synthesis and Application of Organic Functional Molecules, College of Chemistry and Chemical Engineering, Hubei University, Wuhan 430062, PR China. E-mail: zhoulq2003@163.com; zhangsr351@163.com; Fax: +86 27 88663043; Tel: +86 27 88662747*

† Electronic supplementary information (ESI) available. See DOI: 10.1039/c8ra01507d

In this work, we describe the preparation of Ru NPs embedded in MIL-53(Al)-$NH_2$ through an *in situ* impregnation-reduction method. First, the uncoordinated amine groups of MIL-53(Al)-$NH_2$ served as anchoring groups for capturing Ru(III) ions; these amine groups, which are located at the 2-amino-1,4-benzenedicarboxylic acid linkers in MIL-53(Al)-$NH_2$, function as Lewis bases to stabilize $RuCl_3$ during the impregnation process. The strong interaction between the electron lone pair of nitrogen and the d-orbital of the Ru atoms ensure that the formation of Ru NPs is confined to the pores of MIL-53(Al)-$NH_2$ during the reduction process, thereby resulting in the successful embedding of ultra-small Ru NPs in the MIL-53(Al)-$NH_2$. Thus, a catalyst of MIL-53(Al)-$NH_2$ containing embedded Ru NPs was successfully synthesized. PXRD, FT-IR, BET, TEM, EDX, XPS, and ICP-AES measurements were performed to assess the structure, size, morphology, and composition of the Ru/MIL-53(Al)-$NH_2$ catalyst. To compare the turnover frequency (TOF) and activation energy ($E_a$) values of the Ru/MIL-53(Al)-$NH_2$ catalyst with those of the Ru/MIL-53(Al) catalyst in AB hydrolysis, relevant experiments were performed under the same conditions with both catalysts. To provide more insight into the reduction in catalytic activity, durability and reusability tests were performed with both catalysts. To the best of our knowledge, there are no reports of the hydrolysis of AB at room temperature using metal NPs immobilized in an amine-functionalized-MOF with a non-functionalized-MOF for comparison.

# Experimental

### Synthesis of MIL-53(Al)-$NH_2$ and MIL-53(Al)

The preparation of MIL-53(Al)-$NH_2$ was accomplished using a reported method.[21] 2-Amino-1,4-benzenedicarboxylic acid ($NH_2$-BDC) and aluminum nitrate nonahydrate ($Al(NO_3)\cdot 9H_2O$) were used as the organic linker and the metal source, respectively. Typically, 750.3 mg of $Al(NO_3)\cdot 9H_2O$ and 362.3 mg of $NH_2$-BDC were mixed with pure deionized water, and the total volume of solvent was maintained at 5 mL. The reactants were transferred to a 50 mL Teflon-lined stainless steel autoclave and heated at 150 °C for 5 hours. After natural cooling, the resulting yellow products were refluxed in 25 mL of *N*,*N*-dimethylformamide (DMF) at 150 °C for 8 hours to remove residual water or unreacted 2-amino-1,4-benzenedicarboxylic acid molecules trapped in the frameworks of MIL-53(Al)-$NH_2$. After filtering and washing with acetone and ethanol, the resulting yellow products were dried overnight in a vacuum drying oven at 60 °C. MIL-53(Al) was also hydrothermally synthesized according to the reported approach.[22] Typically, the molar ratio of 1,4-benzenedicarboxylic acid, aluminum nitrate nonahydrate, and deionized water was fixed at 0.5 : 1 : 80. The reactants were placed in a 50 mL Teflon-lined stainless steel autoclave and heated at 210 °C for 72 hours. After natural cooling in the autoclave, the resulting white products were obtained by filtration, washed with deionized water, and dried in a vacuum drying oven at 60 °C.

### Synthesis of Ru/MIL-53(Al)-$NH_2$ and Ru/MIL-53(Al) catalysts

In the typical synthesis of the Ru/MIL-53(Al)-$NH_2$ catalyst, 50.0 mg of MIL-53(Al)-$NH_2$ was dispersed in a mixture composed of 10 mL deionized water and 10 mL ethanol in a flask *via* ultrasonication for 10 minutes to obtain a highly dispersed MIL-53(Al)-$NH_2$ suspension. Next, 4, 6, 8, 10 or 12 mL of the solution containing 0.01 M ruthenium(III) chloride ($RuCl_3$) was added to the flask, which was then ultrasonicated for 10 minutes to obtain a uniform dispersion. Magnetic stirring was performed for 5 hours to impregnate the metal salts. Subsequently, 37.8 mg of sodium tetrahydroborate ($NaBH_4$, 1 mM) dissolved in 10 mL deionized water was added dropwise into the uniform dispersion to reduce the Ru(III) ions. After 4 hours of stirring, the resulting solid was obtained through filtration, washed with ethanol and deionized water, and dried overnight in a vacuum drying oven at 60 °C. The Ru/MIL-53(Al) catalyst was synthesized by the same process. For comparison of the catalytic activities, Ru nanoparticles (NPs) without the MIL-53(Al)-$NH_2$ or MIL-53(Al) support were also synthesized through an identical route, and the addition level of Ru (10 mL, 0.01 M $RuCl_3$) was matched to that in the Ru/MIL-53(Al)-$NH_2$(Al) catalyst.

### Catalytic performance

To assess the catalytic activities of the Ru/MIL-53(Al)-$NH_2$ and Ru/MIL-53(Al) catalysts in the dehydrogenation of ammonia borane (AB) aqueous solution, a hydrogen evolution experiment was performed in a two-necked round bottom flask containing 5 mg of the Ru/MIL-53(Al)-$NH_2$ or Ru/MIL-53(Al) catalyst dispersed in 10 mL of deionized water. One neck was connected to a graduated cylinder used to monitor the volume of gas evolved, and the other neck was connected to a pressure-equalization funnel used to introduce 4 mL of the AB (18.5 mg) aqueous solution. The hydrolysis of AB was rapidly initiated upon the addition of the aqueous $NH_3BH_3$ solution to the catalysts, and the displacement of water in the cylinder, which is identical to the volume of generated hydrogen gas, was recorded at constant intervals (15 s). A water bath was employed to maintain reaction temperature at 25 °C. To determine the $E_a$, the hydrolytic experiments were conducted at various temperatures (25, 30, 35, and 40 °C) using the Ru/MIL-53(Al)-$NH_2$ or Ru/MIL-53(Al) catalyst under ambient atmosphere.

To determine the most active Ru loading for Ru/MIL-53(Al)-$NH_2$ in the hydrolysis of AB, a set of experiments with various initial addition levels of Ru/MIL-53(Al)-$NH_2$ ($n$(Ru) = 0.04, 0.06, 0.08, 0.10, 0.12 mmol) were performed at room temperature (25 °C) while maintaining the same amount of AB (18.5 mg), and hydrogen generation was measured. The highest catalytic activity was obtained with the addition of 0.10 mmol Ru in the Ru/MIL-53(Al)-$NH_2$ catalyst. For all the experiments reported hereinafter, the Ru/MIL-53(Al)-$NH_2$ catalyst using 0.10 mmol Ru was tested unless otherwise stated.

### Durability and reusability tests of Ru/MIL-53(Al)-$NH_2$ and Ru/MIL-53(Al) catalysts

For the durability test, the catalytic reaction was repeated 5 times by introducing another equivalent of AB (18.5 mg) into the solution after completion of the previous cycle. For the reusability test, 10 mg of catalyst was employed in the hydrolytic

reaction of AB. The catalysts were collected after each reaction by centrifugation and washed with deionized water three times. Supernatant liquid was decanted, and the isolated catalysts were redispersed in 10 mL deionized water *via* ultrasonication for 10 minutes. Subsequently, a fresh 4 mL of the AB (18.5 mg) aqueous solution was introduced into the reactor containing catalysts redispersed in 10 mL deionized water. The volume of generated hydrogen gas was recorded again.

### Characterization

Powder X-ray diffraction (PXRD) patterns were collected on a Bruker D8-Advance diffractometer (Bruker AXS, Germany) equipped with a Cu K$\alpha$ radiation source ($\lambda$ = 1.5418 Å) with scanning rate at 1° min$^{-1}$ in the 2$\theta$ range of 5–65°. Fourier transform infrared (FT-IR) spectra were collected on an Impact 420 Nicolet instrument (Madison, WI, USA) to determine the structures of the MIL-53(Al)-$NH_2$ and Ru/MIL-53(Al)-$NH_2$ catalysts. Brunauer–Emmett–Teller (BET) specific surface area measurements were performed on $N_2$ sorption isotherms obtained at 77 K using a 2SI-MP-9 instrument (Quantachrome Instruments, America). The morphologies and compositions of the samples were observed using a JEM-2100F (JEOL, Japan) transmission electron microscope (TEM) equipped with an energy dispersive X-ray (EDX) detector at an acceleration voltage of 200 kV. X-ray photoelectron spectroscopy (XPS) was employed to investigate the electronic states of the obtained Ru/MIL-53(Al)-$NH_2$ using ESCALAB 250XI (Thermo Fisher Scientific, America). The actual metal content of the prepared catalysts and the metal leaching of the Ru/MIL-53(Al)-$NH_2$ catalyst in the five consecutive cycles were measured with an IRIS intrepid II XSP (Thermo Fisher Scientific, America) inductively coupled plasma atomic emission spectroscope (ICP-AES).

## Results and discussion

Samples of MIL-53(Al)-$NH_2$, Ru/MIL-53(Al)-$NH_2$, MIL-53(Al), and Ru/MIL-53(Al) were characterized by powder X-ray diffraction (PXRD). As shown in Fig. 1a, the PXRD patterns of MIL-53(Al)-$NH_2$ and MIL-53(Al) agree with the published PXRD results,[21,22] which demonstrates the formation of MIL-53(Al)-$NH_2$ and MIL-53(Al). Additionally, the diffraction peaks of Ru/MIL-53(Al)-$NH_2$(Al) and Ru/MIL-53(Al) samples match well with those of MIL-53(Al)-$NH_2$ and MIL-53(Al), respectively, suggesting that the integrities of the matrix frameworks remained unchanged despite the introduction of a high Ru NP loading. However, the intensities of the peaks decreased substantially as a result of loading Ru NPs into the MOF frameworks.[11] Furthermore, in the magnified PXRD patterns (Fig. 1b) of the Ru/MIL-53(Al)-$NH_2$ and Ru/MIL-53(Al) catalysts, a peak is found at 2$\theta$ = 42.1°, which indicates the presence of Ru in the Ru/MIL-53(Al)-$NH_2$ and Ru/MIL-53(Al) catalysts.

The FT-IR spectra of MIL-53(Al)-$NH_2$, Ru/MIL-53(Al)-$NH_2$, and Ru/MIL-53(Al)-$NH_2$ after the fifth cycle of durability testing are shown in Fig. 2. The two peaks located at 3498.7 and 3382.4 cm$^{-1}$ in MIL-53(Al)-$NH_2$, at 3497.1 and 3388.1 cm$^{-1}$ in Ru/MIL-53(Al)-$NH_2$, and at 3496.9 and 3388.0 cm$^{-1}$ in Ru/MIL-53(Al)-$NH_2$ after durability testing are assigned to the amine groups in the three samples, and the peaks at 1584.3, 1581.1, and 1580.0 cm$^{-1}$ originate from $\delta_{NH}$. In addition, the $\nu_{C=O}$ of DMF (1670.2 cm$^{-1}$) is observed in the spectrum of MIL-53(Al)-$NH_2$,[21] because the DMF molecules trapped in the pores of MIL-53(Al)-$NH_2$ were not completely removed during washing. However, during the preparation of the Ru/MIL-53(Al)-$NH_2$ catalyst, when the salts containing Ru(III) ions and $NaBH_4$ were added, a reduction reaction occurred, and the DMF molecules were replaced by the resulting Ru NPs. Consequently, the $\nu_{C=O}$ from the DMF molecules vanished after the Ru NP loading

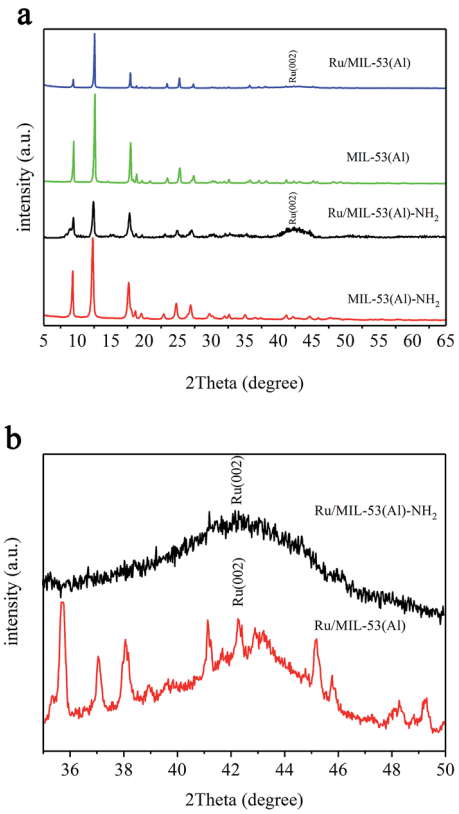


Fig. 1 (a) Wide-angle and (b) magnified Ru PXRD patterns of Ru/MIL-53(Al), MIL-53(Al), Ru/MIL-53(Al)-$NH_2$, and MIL-53(Al)-$NH_2$.

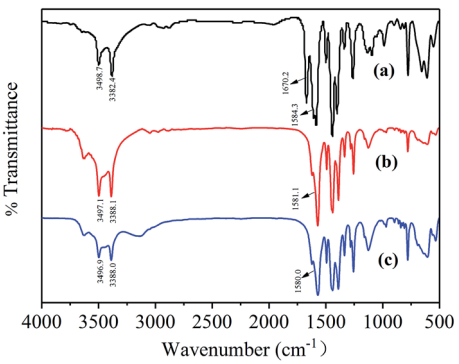


Fig. 2 FT-IR spectra of (a) MIL-53(Al)-$NH_2$, (b) Ru/MIL-53(Al)-$NH_2$, and (c) Ru/MIL-53(Al)-$NH_2$ after the fifth run in the durability test.

process. Compared with the Ru/MIL-53(Al)-$NH_2$, the positions of the main bands of Ru/MIL-53(Al)-$NH_2$ after the fifth run in durability testing show no obvious changes, indicating that the main structure of the Ru/MIL-53(Al)-$NH_2$ remained unchanged.

The $N_2$ sorption isotherms of the MIL-53(Al)-$NH_2$ and Ru/MIL-53(Al)-$NH_2$ samples are shown in Fig. S1a and b.† The Brunauer–Emmett–Teller (BET) specific surface area of MIL-53(Al)-$NH_2$ is 162.4 $m^2\ g^{-1}$, which is approximately the same as previously reported values.[23] Additionally, the pore volume and pore size of MIL-53(Al)-$NH_2$ were measured at 0.8407 $cm^3\ g^{-1}$ and 2.07 nm, respectively (Fig. S1c†). However, the surface area of MIL-53(Al)-$NH_2$ decreased significantly to 57.7 $m^2\ g^{-1}$ after the immobilization of Ru NPs. Accordingly, the pore size decreased from 2.07 to 1.08 nm (Fig. S1d†), and the corresponding pore volume of MIL-53(Al)-$NH_2$ also decreased from 0.8407 to 0.1557 $cm^3\ g^{-1}$. These results indicate that the cavities of MIL-53(Al)-$NH_2$ are either obstructed or occupied by the relatively small Ru NPs, directly decreasing the specific area, pore size, and pore volume.

The morphology and particle size of the Ru/MIL-53(Al)-$NH_2$ catalyst before and after five consecutive cycles were further investigated by transmission electron microscopy (TEM). The TEM images of the initially obtained Ru/MIL-53(Al)-$NH_2$ catalysts (Fig. 3a and b) and those after a fifth run (Fig. 3c and d) clearly show the presence of many ultra-small particles in the matrix, and these NPs are well distributed without agglomeration. As shown in Fig. 3e, the diameters of the Ru NPs in the Ru/MIL-53(Al)-$NH_2$ catalyst have a very narrow size distribution ranging from 0.3 nm to 2.4 nm, and the mean diameter is only 1.22 ± 0.34 nm, which indicates that a large proportion of the Ru NPs are smaller than the mean diameter of the MIL-53(Al)-$NH_2$ pores (2.07 nm). Therefore, Ru NPs were successfully embedded in the frameworks of MIL-53(Al)-$NH_2$, and other larger Ru NPs were supported on the surface. These ultra-small Ru NPs embedded in the MIL-53(Al)-$NH_2$ greatly enhanced the performance of the Ru/MIL-53(Al)-$NH_2$ catalyst.

As shown in Fig. 3c and d, after five catalytic cycles, no obvious changes in the morphology of the Ru/MIL-53(Al)-$NH_2$ catalyst or the uniform distribution of the Ru NPs were observed, and Fig. 3f shows the corresponding particle size distribution of the catalyst after five cycles with a mean diameter of 1.60 ± 0.33 nm. These results confirmed that the crystalline structure of MIL-53(Al)-$NH_2$ remained nearly unchanged after the fifth cycle and that the ultra-small Ru NPs remained immobilized in the frameworks of MIL-53(Al)-$NH_2$. The EDX spectrum shown in Fig. 3g further confirms the presence of Ru in the Ru/MIL-53(Al)-$NH_2$ catalyst. Notably, the peaks at approximately 8 and 9 keV can be attributed to the copper grid.

To investigate the chemical states of the Ru/MIL-53(Al)-$NH_2$ catalyst, X-ray photoelectron spectroscopy (XPS) was performed. Fig. 4a displays the survey XPS spectrum of the prepared Ru/MIL-53(Al)-$NH_2$ catalyst; the main absorption peaks are assigned to C 1s, Ru 3d, Ru 3p, and O 1s. Notably, there is some overlap between the Ru(0) 3d peak and the C 1s peak at approximately 284.7 eV,[24] which can make it difficult to adequately analyze the appropriate region of Ru. Fig. 4b shows that the signals of Ru 3p present two adsorption peaks located at 462.0 eV and 485.1 eV, which are assigned to Ru $3p_{3/2}$ and $3p_{1/2}$, respectively.[25] These results reveal that Ru is stable in the Ru/MIL-53(Al)-$NH_2$ catalyst. The amine groups of MIL-53(Al)-$NH_2$ acted as anchoring groups, and the Ru(III) ions were then reduced to Ru(0) by the $NaBH_4$ reducing agent.

The catalytic performance of Ru/MIL-53(Al)-$NH_2$ with various ICP-AES-authenticated Ru loadings of 11.33, 13.68, 16.69, 18.10,

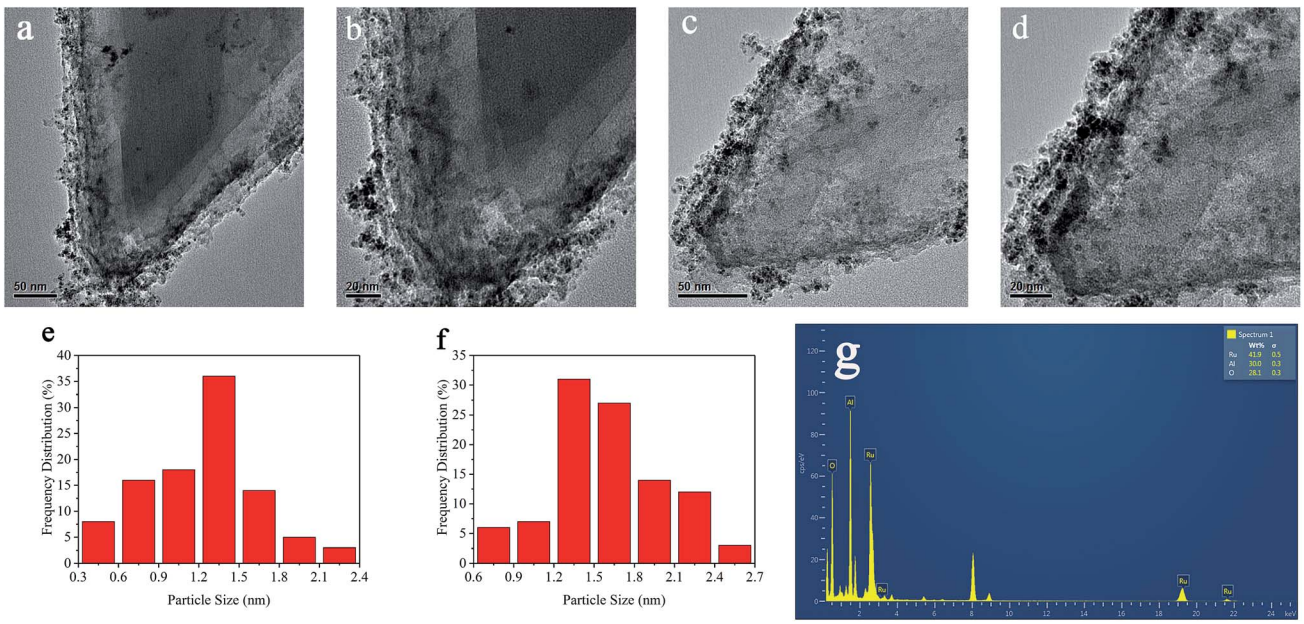


Fig. 3 TEM images of (a and b) initially prepared Ru/MIL-53(Al)-$NH_2$ and (c and d) Ru/MIL-53(Al)-$NH_2$ after five catalytic cycles; particle size distribution of (e) initially prepared Ru/MIL-53(Al)-$NH_2$ and (f) Ru/MIL-53(Al)-$NH_2$ after five catalytic cycles; (g) EDX spectrum of Ru/MIL-53(Al)-$NH_2$.

and 19.42 wt% was compared, and TOF values for these preparations were measured. As shown in Fig. S2 and S3,† the Ru/MIL-53(Al)-$NH_2$ sample with initial Ru addition level of 0.10 mmol displays the highest catalytic activity for the hydrolysis of AB at 25 °C. It is worth noting that the TOF values first increase and then decrease as the initial Ru addition level increases, revealing a volcano-shaped trend (Fig. S3†). This phenomenon can be attributed to the agglomeration of nanoparticles, which leads to a decrease in the accessibility of active sites.[26]

The ICP-AES was also performed on the Ru/MIL-53(Al)-$NH_2$ and Ru/MIL-53(Al) catalysts to determine their authentic Ru loadings. The results showed that the actual content of Ru in the Ru/MIL-53(Al)-$NH_2$ and Ru/MIL-53(Al) catalysts was 18.10 and 12.85 wt%, respectively, although the amount of $RuCl_3$ added to the reaction solution was 0.10 mmol in both cases. Thus, the actual Ru loading in the Ru/MIL-53(Al)-$NH_2$ catalyst far exceeds that in the Ru/MIL-53(Al) catalyst. A plausible explanation is that the majority of Ru(III) ions were adsorbed by the amine groups in the MIL-53(Al)-$NH_2$ framework. The higher Ru loading catalytic performance for the Ru/MIL-53(Al)-$NH_2$ catalyst compared with the Ru/MIL-53(Al) catalyst.

The catalytic activities of the prepared Ru/MIL-53(Al)-$NH_2$ and Ru/MIL-53(Al) catalysts in the hydrolysis of AB were systematically evaluated at 25 °C. To compare the catalytic performances, the same amount of Ru NPs was synthesized through reduction by $NaBH_4$ without the MIL-53(Al)-$NH_2$ or MIL-53(Al) support and utilized in the hydrolysis of AB. As shown in Fig. 5, MIL-53(Al)-$NH_2$ and MIL-53(Al) exhibited no catalytic activity toward the dehydrogenation of AB aqueous solution, whereas the reaction time for the complete hydrogen release (mol $H_2$/mol AB = 3.0) was more than 10 minutes for the same amount of Ru NPs lacking the matrix. Additionally, the Ru/MIL-53(Al)-$NH_2$ catalyst displayed superior catalytic activity compared with the Ru/MIL-53(Al) and Ru NPs catalysts: the Ru/MIL-53(Al)-$NH_2$ catalyst with a Ru content of 18.10 wt% exhibited the highest TOF value of 287 mol $H_2$ $min^{-1}$ (mol Ru)$^{-1}$. In contrast, a TOF value of 218 mol $H_2$ $min^{-1}$ (mol Ru)$^{-1}$ was calculated for the Ru/MIL-53(Al) catalyst, which generally agrees with previously reported values.[27] Therefore, the TOF value of the Ru/MIL-53(Al)-$NH_2$ catalyst is much larger than that of the Ru/MIL-53(Al) in this study. Moreover, this value is higher than those of most Ru-based catalysts, which are illustrated in Table 1. These experimental results reveal that the bifunctional effects of the Ru NPs and the MIL-53(Al)-$NH_2$ framework dramatically increased the catalytic activity of the Ru/MIL-53(Al)-$NH_2$ catalyst; MIL-53(Al)-$NH_2$ offers an excellent framework for Ru NPs even though it does not participate in the AB hydrolysis. Additionally, the ultra-small size of the Ru NPs and the higher authentic Ru loading in the Ru/MIL-53(Al)-$NH_2$ catalyst, both of which result from the presence of amine groups in the framework of MIL-53(Al)-$NH_2$, contribute to this excellent catalytic performance. More importantly, these results also show that MIL-53(Al)-$NH_2$ is superior to MIL-53(Al) as a matrix for the Ru NPs.

The catalytic reaction appears to occur on the exterior of the metal catalyst.[37] A plausible two-step catalytic mechanism for the hydrolytic reaction is proposed as follows. First, AB interacts with the exterior of the Ru nanoparticles to form a transient activated Ru–H species, which is accepted to be a precondition for the hydrolytic reaction. Then, $H_2$ is generated after the attack of $H_2O$ molecules on the Ru–H species.[38] Because the amine groups could be used as anchoring groups to stabilize the Ru NPs, ultra-small and well-distributed NPs could be supported on the surface of the framework, which leads to a significant enhancement of surface contact among the Ru NPs and AB and an increase in the number of active sites that could form the activated transient Ru–H species. Consequently, a higher hydrogen generation rate and productivity were noted

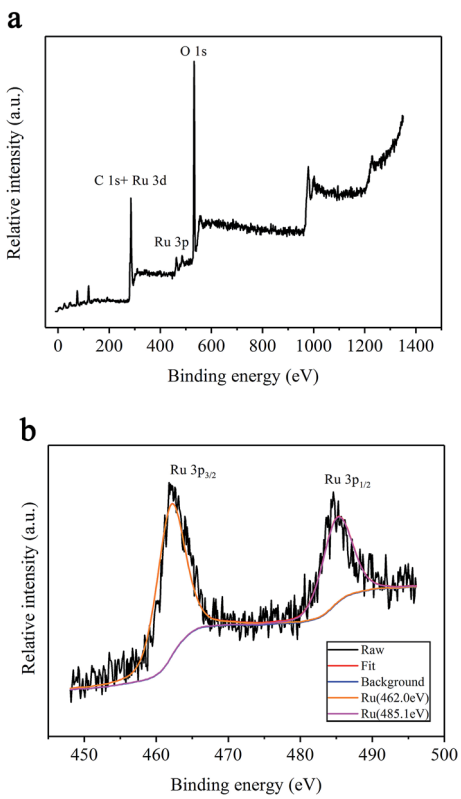


Fig. 4 XPS spectra of the synthesized Ru/MIL-53(Al)-$NH_2$ catalyst: (a) survey scan and (b) Ru 3p spectrum.

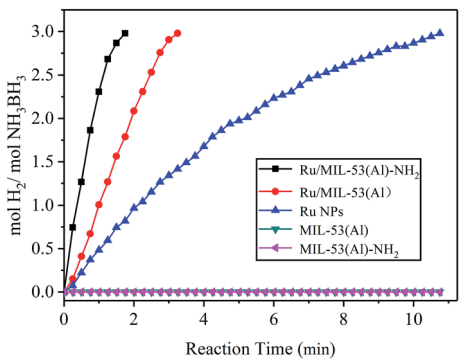


Fig. 5 Hydrogen generation from the hydrolysis of AB catalyzed by Ru/MIL-53(Al)-$NH_2$, Ru/MIL-53, Ru NPs, MIL-53(Al), and MIL-53(Al)-$NH_2$.

Table 1 Catalytic activities of different Ru-based catalysts used for the hydrolytic dehydrogenation of AB

| Catalyst | TOF (mol $H_2$ $mol^{-1}$ Ru $min^{-1}$) | $E_a$ (kJ $mol^{-1}$) | ln $A$ | Temperature range (°C) | Ref. |
|---|---|---|---|---|---|
| Ru@Ni | 339.5 | 36.59 | 26.55 | 25–40 | 28 |
| RuCuNi/CNTs | 311.15 | 36.67 | 34.27 | 25–40 | 29 |
| Ru/MIL-53(Al)-$NH_2$ | 287 | 30.5 | 11.3 | 25–40 | This study |
| Ru/MIL-53(Al) | 218 | 37.2 | 13.4 | 25–40 | This study |
| RuCuCo@MIL-101 | 241.2 | 48 | 36.91 | 25–40 | 19 |
| Ru/ND | 229 | 50.7 | — | 20–35 | 30 |
| Ru@$SiO_2$ | 200 | 38.2 | 18.2 | 20–45 | 31 |
| Ru(0)/$SiO_2$-$CoFe_2O_4$ | 172 | 45.6 | 20.7 | 25–40 | 32 |
| $Ru^0/HfO_2$ | 170 | 65 | — | 25–40 | 33 |
| Ru(0)@X-NW | 135 | 77 | 30.24 | 20–40 | 34 |
| CuRu@C-1b | 97 | 39.2 | — | 20–50 | 35 |
| Ru@$Al_2O_3$ | 83.3 | 48 | 23.6 | 25–40 | 36 |

for the Ru/MIL-53(Al)-$NH_2$ catalyst relative to the Ru/MIL-53(Al) catalyst.

To determine the $E_a$ of the AB hydrolytic reaction catalyzed by the Ru/MIL-53(Al)-$NH_2$ catalyst, the hydrolytic reactions were performed at various temperatures ranging from 25 °C to 40 °C. The apparent $E_a$ values for the hydrolysis of AB over the Ru/MIL-53(Al)-$NH_2$ and Ru/MIL-53(Al) catalysts were determined from the Arrhenius equation (1), in which $k$ stands for the rate constant, and $A$ and $R$ represent the pre-exponential factor and gas constant, respectively. Fig. 6a and c indicate that the hydrolytic rates for both the Ru/MIL-53(Al)-$NH_2$ and Ru/MIL-53(Al) catalysts increased with increasing temperature, and the values of the rate constant $k$ for the hydrolytic reaction of AB were determined based on the slopes of the fitted lines and then were used to measure $E_a$. The Arrhenius plot of ln $k$ *vs.* $1/T$ for the Ru/MIL-53(Al)-$NH_2$ catalyst is plotted in Fig. 6b, and the $E_a$ for the hydrolytic reaction of AB was calculated as approximately 30.5 kJ $mol^{-1}$. Fig. 6d shows an $E_a$ for Ru/MIL-53(Al) of 37.2 kJ $mol^{-1}$, which is approximately the same as previously reported values.[27] Thus, the $E_a$ of the Ru/MIL-53(Al)-$NH_2$ catalyst is obviously lower than that of Ru/MIL-53(Al) in this study. From the comparison of the catalytic activities and activation energies of other Ru-based catalysts provided in Table 1, the Ru/MIL-53(Al)-$NH_2$ catalyst exhibited a low $E_a$ and an excellent catalytic performance due to the strong bifunctional effects between the Ru NPs and the MIL-53(Al)-$NH_2$ matrix and the uniform

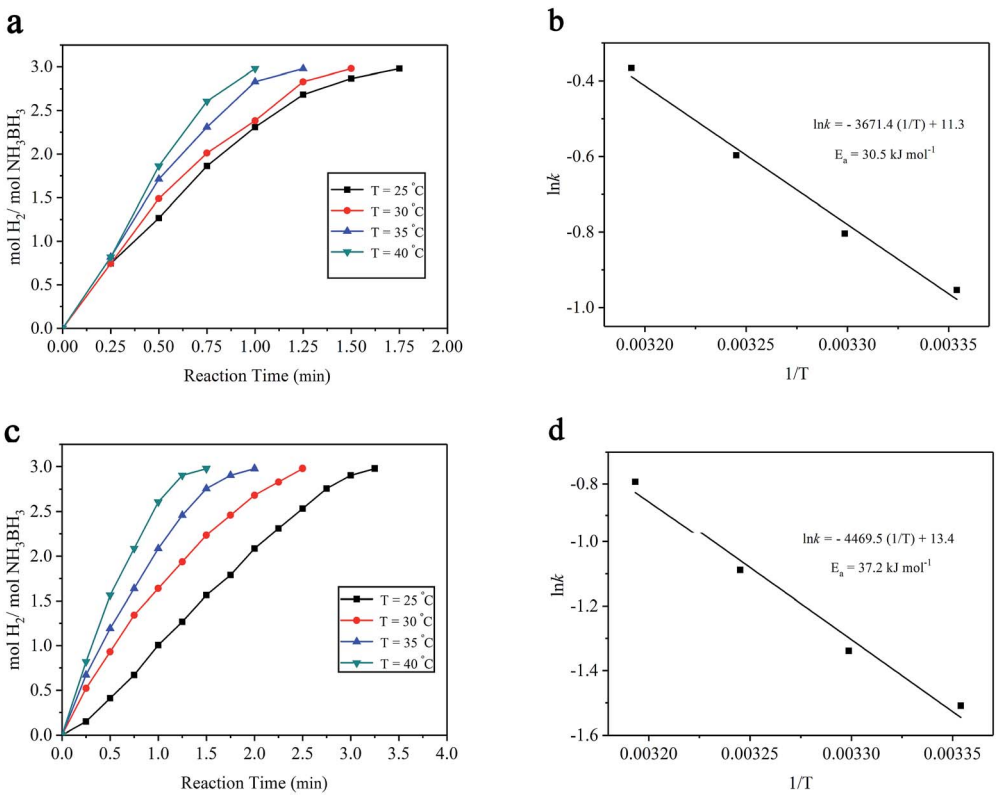


Fig. 6 (a and c) Effect of temperature on the hydrogen generation rate catalyzed by Ru/MIL-53(Al)-$NH_2$ and Ru/MIL-53(Al) catalysts; (b and d) Arrhenius plots obtained from the corresponding temperature effects.

distribution of ultra-small Ru NPs. These results show that the Ru/MIL-53(Al)-$NH_2$ catalyst is a good candidate for the dehydrogenation of AB aqueous solution.

$$\ln k = \ln A - E_a/RT \quad (1)$$

In general, the higher the rate constant ($k$), the higher the TOF. According to the Arrhenius equation (1), the activation energy ($E_a$) and the pre-exponential factor ($A$) have significant influence on the rate constant ($k$). The activation energy ($E_a$) depends on the mechanism of the catalytic reaction, which has a major impact on the rate constant ($k$) because it determines the slope in the Arrhenius equation (1). In contrast, the pre-exponential factor ($A$) depends on the number of active sites and has a minor impact on the rate constant ($k$) because it determines the intercept in the Arrhenius equation (1). Thus, top priority should be given to reducing the activation energy ($E_a$) to obtain high TOF values. Thus, the lower the activation energy ($E_a$) is, the higher the TOF value of catalysts, as shown in Table 1. However, in recent years, some studies have shown that when there is little difference between two catalysts' activation energy ($E_a$), the difference in the rate constant ($k$) is entirely due to the variation in the number of active sites, which determine the values of the pre-exponential factor ($A$).[39] In conclusion, the lower the activation energy ($E_a$) and the higher the pre-exponential factor ($A$), the greater the contribution to TOF values.

Durability studies of a catalyst are essential for its practical application. Thus, the stability of the catalyst in the hydrolytic reaction of AB was investigated, as shown in Fig. 7a and c. For the durability test, the catalytic reactions were repeated five times by introducing additional equivalents of AB (18.5 mg) into the mixture after a previous cycle. The definition of loss in catalytic activity is defined as the percentage drop in initial activity based on the slopes of the linear portion of each plot shown in Fig. 7a and c. As shown in Fig. 7b, the Ru/MIL-53(Al)-$NH_2$ catalyst retained approximately 87.6% of its initial catalytic activity in the second cycle of AB hydrolysis, and 82.1%, 79.1%, and 72.4% of initial activity was retained, respectively, in subsequent cycles. Considering that only 5 mg of catalyst was utilized in the reaction, the performance of this catalyst is impressive. In contrast to the Ru/MIL-53(Al)-$NH_2$ catalyst, the Ru/MIL-53(Al) catalyst maintained approximately 64.3% of its initial catalytic activity in the fifth cycle, as shown in Fig. 7d.

To provide more insight into the reduction in catalytic activity, reusability tests were performed with Ru/MIL-53(Al)-$NH_2$ and Ru/MIL-53 catalysts. The definition of loss in catalytic

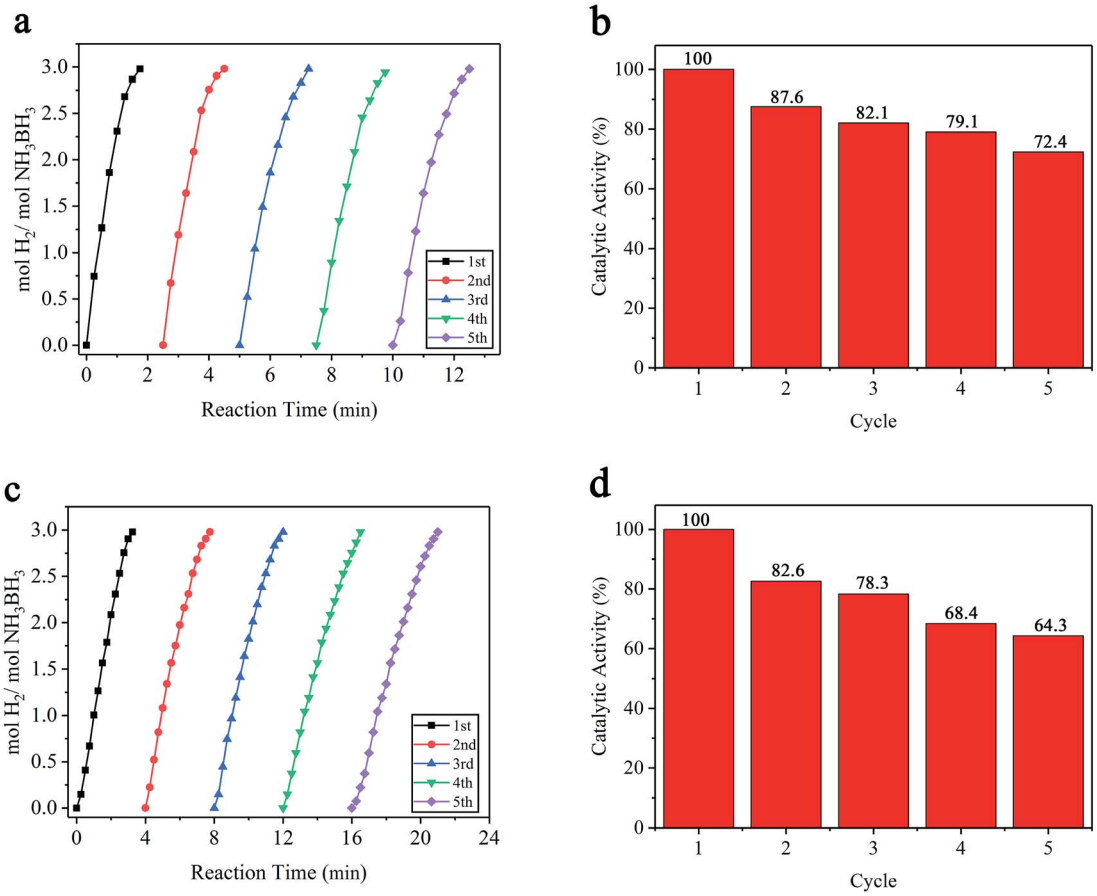


Fig. 7 (a and c) Durability of Ru/MIL-53(Al)-$NH_2$ and Ru/MIL-53(Al) catalysts from the 1st to the 5th cycle; (b and d) corresponding percentage of the initial catalytic activity remaining after successive cycles of AB hydrolysis.

activity is the same as the durability test. After the completion of each cycle, the solid catalyst was recovered by centrifugation, and the supernatant liquid was decanted. Then, catalysts were washed with deionized water three times and redispersed in deionized water for the next cycle. Fig. 8b and d show the percentages of initial catalytic activity for Ru/MIL-53(Al)-$NH_2$ and Ru/MIL-53 catalysts in subsequent cycles by using catalysts isolated after each preceding hydrolysis cycle at 25 °C. After the fifth cycle in the reusability tests, Ru/MIL-53(Al)-$NH_2$ and Ru/MIL-53 catalysts retained 86.3% and 77.5% of their initial catalytic activity, respectively, for AB hydrolysis. Therefore, the performance of Ru/MIL-53(Al)-$NH_2$ in the reusability test is remarkable. It is obvious that the catalysts have better performance in reusability tests than in durability tests and that Ru/MIL-53(Al)-$NH_2$ is more durable and reusable than Ru/MIL-53(Al). These results reveal that the observed decreases of catalytic activity are mainly attributable to the increasing viscosity of the reaction solution and the deactivation effect caused by the increasing metaborate concentration that many studies have reported.[40,41] To be more specific, the increasing viscosity of the solution after multiple cycles may impede the diffusion of AB, obstructing the interaction between the Ru NPs and AB, thus resulting in decreased catalytic activity. In addition, the increasing metaborate can be absorbed on the Ru NP surface and cover active sites. Furthermore, as shown in Fig. 3e and f, the Ru particle size increased from 1.22 to 1.60 nm after the fifth durability test, and the increase of Ru particle size can contribute to the decrease of the catalytic activity reported in many studies.[30,42] In some reports, metal leaching may have also led to the decline in the catalytic activity.[43] Generally, metal leaching depends upon the reaction medium (pH, oxidation potential, and chelating properties of the metal) and the bulk and surface properties of the metal.[44] Moreover, if the Ru nanoparticles detached from the support, they can easily aggregate in solution, thus resulting in decreased catalytic activity.[45] In the durability test, the amount of metal Ru that leached from the Ru/MIL-53(Al)-$NH_2$ catalyst in the five cycles was determined to be 0.75%, 1.05%, 1.33%, 1.46%, and 1.64%, respectively (see Table 2). Note that this amount of leached metal for the Ru/MIL-53(Al)-$NH_2$ catalyst is very low, indicating that the Ru NPs remain effectively embedded in the MIL-53(Al)-$NH_2$ host. Additionally, representative TEM images of Ru/MIL-53(Al)-$NH_2$ after the fifth durability test also showed that no obvious changes occurred in the morphology or uniform distribution of the Ru NPs (Fig. 3c and d). These results reveal that the amine groups in the MIL-53(Al)-$NH_2$ matrix act as anchoring groups to capture Ru(III) ions and stabilize ultrasmall Ru NPs, effectively preventing their aggregation and thus resulting in superior performance in durability and reusability tests.

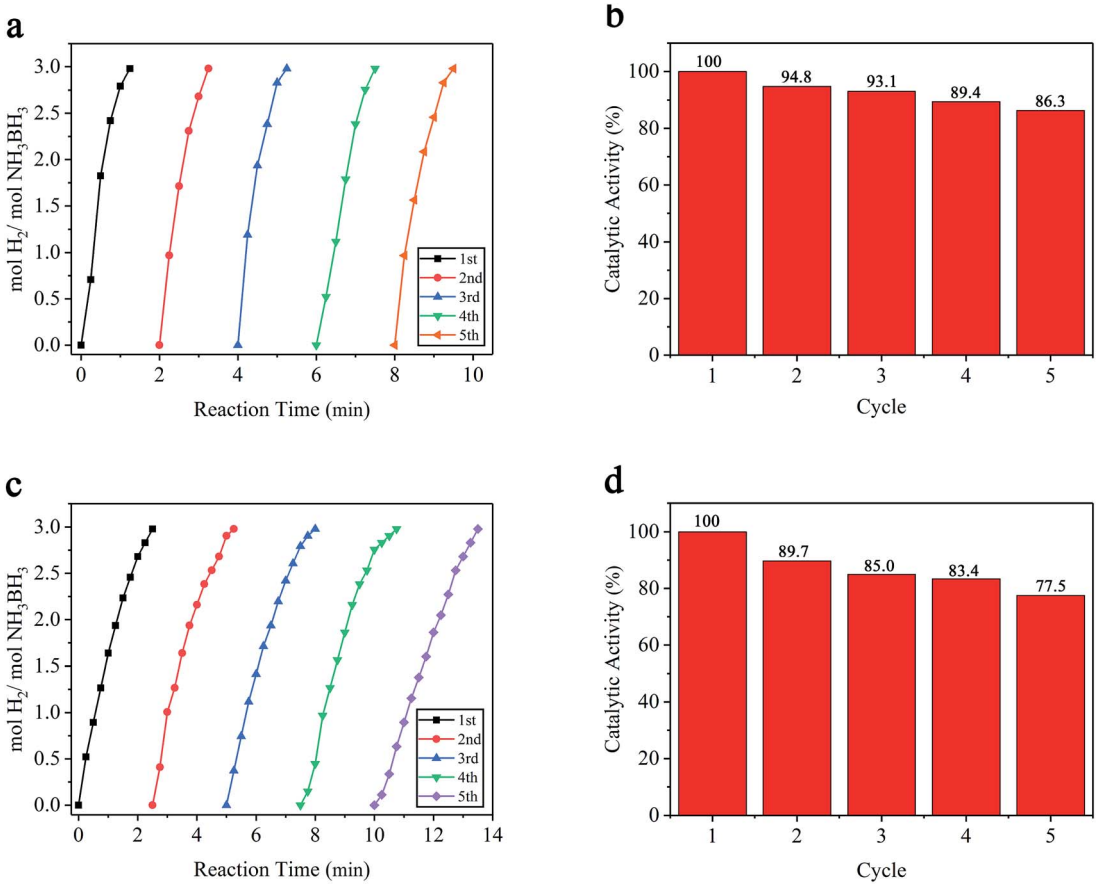


Fig. 8 (a and c) Reusability of the Ru/MIL-53(Al)-$NH_2$ and Ru/MIL-53(Al) catalysts from the 1st to the 5th cycle; (b and d) corresponding percentage of the initial catalytic activity remaining after successive cycles of AB hydrolysis.

Table 2 Metal leaching of Ru/MIL-53(Al)-$NH_2$ (5 mg) in successive cycles of AB hydrolysis

| Run | Ru leaching (mg) | Metal leaching (%) |
|---|---|---|
| 1 | 0.0068 | 0.75% |
| 2 | 0.0095 | 1.05% |
| 3 | 0.0121 | 1.33% |
| 4 | 0.0132 | 1.46% |
| 5 | 0.0149 | 1.64% |

## Conclusions

In summary, the ultra-small Ru NPs embedded in the MIL-53-$NH_2$ matrix exhibited a much higher catalytic activity and lower $E_a$ for hydrogen generation from AB at ambient temperature compared with Ru NPs embedded in MIL-53. Furthermore, the Ru/MIL-53(Al)-$NH_2$ catalyst was recyclable in the hydrolytic reaction of AB, preserving 72.4% and 86.3% of its initial activity in the durability test and reusability test after the fifth cycle, respectively. The main property leading to the excellent catalytic performance was the presence of amine groups in the MIL-53-$NH_2$ framework, which stabilized the Ru NPs and maintained their ultra-small size and good distribution. Therefore, the Ru/MIL-53(Al)-$NH_2$ catalyst is a promising candidate for application in the development of AB as a highly efficient and portable hydrogen storage system. The present work indicates that amine functionalization of the MOF material substantially improved the catalytic performance of the catalyst, and this strategy can easily be extended to other functionalized MOFs and metal NPs.

## Conflicts of interest

There are no conflicts to declare.

## Acknowledgements

This project was sponsored by the Natural Science Fund for Creative Research Groups of Hubei Province (2014CFA015) and the Hubei Province Education Office Key Laboratory (2016-KL-007) of China. This work was also sponsored by the Hubei College Students' Innovation Training Program of China (201510 512030).

## Notes and references

1 P. Jena, *J. Phys. Chem. Lett.*, 2011, **2**, 206–211.
2 S. Akbayrak, Y. Tonbul and S. Ozkar, *Dalton Trans.*, 2016, **45**, 10969–10978.
3 U. Eberle, M. Felderhoff and F. Schuth, *Angew. Chem., Int. Ed.*, 2009, **48**, 6608–6630.
4 B. Roy, J. Manna and P. Sharma, *J. Alloys Compd.*, 2015, **645**, 234–238.
5 H. Wang, L. Zhou, M. Han, Z. Tao, F. Cheng and J. Chen, *J. Alloys Compd.*, 2015, **651**, 382–388.
6 L. Yang, J. Su, X. Meng, W. Luo and G. Cheng, *J. Mater. Chem. A*, 2013, **1**, 10016–10023.
7 L. Wen, J. Su, X. Wu, P. Cai, W. Luo and G. Cheng, *Int. J. Hydrogen Energy*, 2014, **39**, 17129–17135.
8 S. Sorribas, B. Zornoza, P. Serra-Crespo, J. Gascon, F. Kapteijn, C. Téllez and J. Coronas, *Microporous Mesoporous Mater.*, 2016, **225**, 116–121.
9 R. Huxford, J. Della Rocca and W. Lin, *Curr. Opin. Chem. Biol.*, 2010, **14**, 262.
10 T. T. Dang, Y. Zhu, J. S. Y. Ngiam, S. C. Ghosh, A. Chen and A. M. Seayad, *ACS Catal.*, 2013, **3**, 1406.
11 H. R. Moon, D. W. Lim and M. P. Suh, *Chem. Soc. Rev.*, 2013, **42**, 1807–1824.
12 T. Gadzikwa, O. K. Farha, K. L. Mulfort, J. T. Hupp and S. T. Nguyen, *Chem. Commun.*, 2009, 3720–3722.
13 S. J. Garibay and S. M. Cohen, *Chem. Commun.*, 2010, **46**, 7700–7702.
14 K. Koh, J. E. Seo, J. H. Lee, A. Goswami, C. W. Yoon and T. Asefa, *J. Mater. Chem. A*, 2014, **2**, 20444–20449.
15 M. J. Ingleson, J. Perez Barrio, J.-B. Guilbaud, Y. Z. Khimyak and M. J. Rosseinsky, *Chem. Commun.*, 2008, 2680–2682.
16 R. J. White, R. Luque, V. L. Budarin, J. H. Clark and D. J. Macquarrie, *Chem. Soc. Rev.*, 2009, **38**, 481–494.
17 Z. H. Lu, J. P. Li, G. Feng, Q. L. Yao, F. Zhang, R. Y. Zhou, D. J. Tao, X. S. Chen and Z. Q. Yu, *Int. J. Hydrogen Energy*, 2014, **39**, 13389–13395.
18 D. Lu, G. Yu, Y. Li, M. Chen, Y. Pan, L. Zhou, K. Yang, X. Xiong, P. Wu and Q. Xia, *J. Alloys Compd.*, 2017, **694**, 662–671.
19 K. Yang, L. Zhou, X. Xiong, M. Ye, L. Li and Q. Xia, *Microporous Mesoporous Mater.*, 2016, **225**, 1–8.
20 D. Sun, P. Li, B. Yang, Y. Xu, J. Huang and Q. Li, *RSC Adv.*, 2016, **6**, 105940–105947.
21 T. Ahnfeldt, D. Gunzelmann, T. Loiseau, D. Hirsemann, J. Senker, G. Ferey and N. Stock, *Inorg. Chem.*, 2009, **48**, 3057–3064.
22 T. Loiseau, C. Serre, C. Huguenard, G. Fink, F. Taulelle, M. Henry, T. Bataille and G. Férey, *Chemistry*, 2004, **10**, 1373.
23 L. Liu, X. Tai, X. Zhou and L. Liu, *Chem. Res. Chin. Univ.*, 2017, **33**, 231–238.
24 S. Akbayrak, P. Erdek and S. Ozkar, *Appl. Catal., B*, 2013, **142**, 187–195.
25 M. Rakap, *J. Alloys Compd.*, 2015, **649**, 1025–1030.
26 S. Akbayrak and S. Özkar, *ACS Appl. Mater. Interfaces*, 2012, **4**, 6302–6310.
27 K. Yang, L. Zhou, G. Yu, X. Xiong, M. Ye, Y. Li, D. Lu, Y. Pan, M. Chen and L. Zhang, *Int. J. Hydrogen Energy*, 2016, **41**, 6300–6309.
28 C. Nan, J. Su, L. Wei and G. Cheng, *Int. J. Hydrogen Energy*, 2014, **39**, 426–435.
29 X. Xiong, L. Zhou, G. Yu, K. Yang, M. Ye and Q. Xia, *Int. J. Hydrogen Energy*, 2015, **40**, 15521–15528.
30 G. Fan, Q. Liu, D. Tang, X. Li, J. Bi and D. Gao, *Int. J. Hydrogen Energy*, 2016, **41**, 1542–1549.
31 Q. L. Yao, W. M. Shi, G. Feng, Z. H. Lu, X. L. Zhang, D. J. Tao, D. J. Kong and X. S. Chen, *J. Power Sources*, 2014, **257**, 293–299.

 

32 S. Akbayrak, M. Kaya, M. Volkan and S. Özkar, *J. Mol. Catal. A: Chem.*, 2014, **394**, 253–261.
33 E. B. Kalkan, S. Akbayrak and S. Özkar, *J. Mol. Catal. A: Chem.*, 2017, **430**, 29–35.
34 S. Akbayrak and S. Ozkar, *Dalton Trans.*, 2014, **43**, 1797–1805.
35 P. Pachfule, X. Yang, Q.-L. Zhu, N. Tsumori, T. Uchida and Q. Xu, *J. Mater. Chem. A*, 2017, **5**, 4835–4841.
36 H. Can and O. Metin, *Appl. Catal., B*, 2012, **125**, 304–310.
37 D. D. Ke, Y. Li, J. Wang, L. Zhang, J. D. Wang, X. Zhao, S. Q. Yang and S. M. Han, *Int. J. Hydrogen Energy*, 2016, **41**, 2564–2574.
38 Q. Xu and M. Chandra, *J. Power Sources*, 2006, **163**, 364–370.
39 X. W. Xie, Y. Li, Z. Q. Liu, M. Haruta and W. J. Shen, *Nature*, 2009, **458**, 746–749.
40 M. Rakap and S. Ozkar, *Int. J. Hydrogen Energy*, 2010, **35**, 3341–3346.
41 Ö. Metin, Ş. Şahin and S. Özkar, *Int. J. Hydrogen Energy*, 2009, **34**, 6304–6313.
42 N. Cao, W. Luo and G. Z. Cheng, *Int. J. Hydrogen Energy*, 2013, **38**, 11964–11972.
43 D. D. Gao, Y. H. Zhang, L. Q. Zhou and K. Z. Yang, *Appl. Surf. Sci.*, 2018, **427**, 114–122.
44 M. Besson and P. Gallezot, *Catal. Today*, 2003, **81**, 547–559.
45 H. Liang, G. Chen, S. Desinan, R. Rosei, F. Rosei and D. Ma, *Int. J. Hydrogen Energy*, 2012, **37**, 17921–17927.